Eur. Phys. J. Plus (2023) 138:827
https://doi.org/10.1140/epjp/s13360-023-04462-8

THE EUROPEAN PHYSICAL JOURNAL PLUS

Regular Article

Gold coated microstructures as a platform for the preparation of semiconductor-based hybrid 3D micro-nano-architectures

Eduard V. Monaico[1,a], **Veaceslav V. Ursaki**[1,2,b], **Ion M. Tiginyanu**[1,2,c]

[1] National Center for Materials Study and Testing, Technical University of Moldova, 2004 Chisinau, Moldova
[2] Academy of Sciences of Moldova, 2001 Chisinau, Moldova

Received: 1 May 2023 / Accepted: 9 September 2023

Abstract In this paper, three types of microstructures are argued as substrates for electrochemical deposition of Au nanodots. They include: (a) aero-GaN consisting of hollow GaN microtetrapods, (b) microdomains of pores with a controlled design produced by anodization of InP wafers, and (c) patterned microdomains composed of strips with alternating electrical conductivity in GaN crystals grown by hydride vapor phase epitaxy. Uniform deposition of Au nanodots with controlled density is demonstrated by using pulsed electroplating, the voltage pulse width and amplitude as well as the pause between pulses and the conductivity of the substrate serving as adjustable parameters. The morphology of the produced hybrid microarchitectures was investigated by scanning electron microscopy. The explored microstructures are proposed as platforms for the development of complex 3D hybrid micro-nano-architectures via the vapor–liquid–solid deposition of various semiconductor nanowires with Au nanodots as catalysts.

1 Introduction

Various functional nanowires with bandgap covering the spectral range from near infrared (NIR) to ultraviolet (UV) have been grown on a variety of semiconductor substrates by means of catalyst-assisted or self-catalyzed vapor–liquid–solid (VLS) processes. In the catalyst-assisted processes, Au is the most frequently used catalyzer. As concerns the technologies applied in the VLS process, they include molecular beam epitaxy (MBE), chemical vapor deposition (CVD), plasma enhanced chemical vapor deposition (PECVD), metalorganic vapor phase epitaxy (MOVPE) or metal organic chemical vapor deposition (MOCVD) and hydride vapor phase epitaxy (HVPE).

InP and GaAs nanowires belong to semiconductor materials with the bandgap in the NIR spectral range. They have been produced both with Au catalyst and by self-catalyzed VLS process on various substrates. InP nanowires have been grown with In droplets in the self-catalyzed VLS process on Si substrates by MOCVD technology [1] and on InP substrates by MOVPE method [2]. With Au catalyst, InP nanowires have been grown by MOVPE technology on InP [3], MoS_2 [4], and quartz [5] substrates. InP nanowires have also been grown by MBE with Au-In droplets as catalyst on Si substrates [6]. Apart from pure InP nanowires, InAs/InP quantum rod nanowires were grown on Si substrate [7], InAs/InP quantum-disk nanowires were grown on InP substrates [8], and alternating InAsP/InP heterostructure nanowires with multiple-quantum-dot structures were grown on InP substrates [9] with Au catalyst. InP nanowire stems with InSb nanoflags have been grown with Au catalyst for quantum devices [10].

GaAs nanowires have been grown with Ga droplets in the self-catalyzed VLS process on Si substrates by MBE technology [11–13]. With Au catalyst, GaAs nanowires have been grown by HVPE technology on GaAs [14], by MOVPE technology on GaN [15], and by MOCVD technology on SiN [16] substrates. Apart from pure GaAs nanowires, axial GaAs/Ga(As, Bi) heterostructures were grown on Si substrates [17], GaAs/(InGa)As/GaAs axial double-heterostructure nanowires [18], core–shell GaAs-AlGaAs nanowires [19] and GaAs/GaSb core–shell heterostructured nanowires [20] were grown on GaAs substrates, and InAs/GaAs core–shell nanowires were grown on InAs substrates [21] with Au catalyst.

GaP nanowires with the bandgap in the visible spectral range have been grown with Ga catalyst in the self-catalyzed VLS process on Si substrates by MBE technology [22]. With Au catalyst, GaP nanowires have been grown by MOVPE [23] and by MBE technologies [24] on Si substrates, as well as by MOVPE [25] and by solid-source sublimation method [26] on GaP substrates. Apart from pure GaP nanowires, axial hybrid GaP/Si nanowires [27] and core–shell GaP/GaPN nanowires [28] were grown on GaP substrates with Au catalyst.

[a] e-mail: eduard.monaico@cnstm.utm.md (corresponding author)
[b] e-mail: vvursaki@gmail.com
[c] e-mail: tiginyanu@asm.md

Published online: 21 September 2023

GaN, ZnO, and ZnS nanowire structures were grown for the UV spectral range applications. GaN nanowires were grown with Ga droplets in the self-catalyzed VLS process on Si substrates using CVD technology [29]. With Ga-Au-In alloy catalyst, GaN nanowires were grown by MOCVD on GaN and sapphire substrates [30]. With Ni catalyst, GaN nanowires were grown by CVD on sapphire substrates [31]. HVPE technology was applied to grow GaN nanowires on Si substrates with either Au catalyst [32], or with Ni-Au catalyst [33]. In addition to pure GaN nanowires, GaN/InGaN core/shell multiple quantum well (MQW) co-axial heterostructure nanowires were grown on a variety of sapphire, silicone, copper, tungsten, glass, gallium nitride, and beryllium oxide substrates [34]. ZnO nanowires were grown with Au catalyst by carbothermal reduction method on Si substrates [35, 36], by vapor phase deposition [37] and by mist-CVD [38] on GaN substrates. In addition to pure ZnO nanowires, ZnO-ZnMgO core–shell nanowires have been grown on sapphire with Au catalysts [39]. ZnS nanowires [40, 41] and ZnS nanotubes [42] were grown by thermal evaporation of ZnS powder on Si substrates with Au catalysts. ZnS nanowires were also grown by MOCVD on GaAs substrates with Au catalysts [43]. Apart from pure ZnS nanowires, ZnS/diamond-like carbon (DLC) core–shell heterostructure nanowires [44] and ZnS/SiO_2 core–shell nanowires [45] were fabricated on Si substrates with Au catalysts. GaN/ReS_2, ZnS/ReS_2 and ZnO/ReS_2 core–shell nanowire heterostructures were produced by CVD on SiO_2/Si wafers with Au catalysts [46].

The variety of semiconductor nanowire structures produced with Au catalyst-assisted VLS growth on various substrates, covering a wide spectral range, constitutes a powerful platform for many applications in electronics, optoelectronics, photonics, energy, photocatalysis, piezoelectric generators, sensors etc. At the same time, most of these nanostructures were prepared on flat substrates. Deposition of semiconductor nanowire arrays on microstructures with controlled design and morphology, would result in more complex micro-nano-structure assemblies, which are expected to enlarge even more their areas of applications.

The goal of this paper is to demonstrate some 3D microstructure platforms with Au nanodot coatings for subsequent growth of semiconductor nanowires and other applications.

2 Methods and materials

Three basic types of substrates were used in this paper. The first one is composed of aero-GaN 3D structures obtained by transforming the sacrificial ZnO tetrapods [47] into GaN microtubes in a HVPE process as described elsewhere [48].

The second type of substrates was prepared on crystalline 500-μm thick *n*-InP(100) wafers with a free electron concentration of 1.3×10^{18} cm^{-3} supplied by CrysTec GmbH, Germany. Anodization was performed using 3.5 M NaCl electrolyte in the potentiostatic mode at applied voltage of $U = +6$ V in a double electrochemical cell with three electrodes, where the InP wafer played the role of working electrode, while an Ag/AgCl electrode and a Pt electrode served as reference and counter electrode, respectively.

Free-standing HVPE-grown 300-μm thick wurtzite-phase (0001)-orientated *n*-GaN single crystalline samples with the density of threading dislocations in the range $(1–2) \times 10^{7}$ cm^{-2} acquired from SAINT-GOBAIN Crystals served as a third type of substrates.

Pulsed electrochemical deposition of Au was realized in a commercially available gold bath containing 5 g L^{-1} Au (DODUCO GmbH, Germany) at temperature of 25 °C in a common two-electrode plating cell where the sample served as working electrode, while a platinum wire was used as a counter electrode. The electrochemical etching and pulsed electroplating with controlled parameters of pulse width (t_{on}), pause between pulses (t_{off}), and voltage pulse amplitude (U) were performed according to the experimental setup and methodology described in detail in a recent paper [49]. In the case of electroplating on aero-GaN pellets, half of the sample was immersed in plating electrolyte, while the electrical contact was realized on the other side by means of silver paste.

The morphology (top view and cross-sectional view) of samples was investigated using TESCAN Vega TS 5130 MM scanning electron microscope (SEM).

3 Results and discussions

3.1 Aero-GaN covered by Au nanodots

Various aeromaterials consisting of hollow microtetrapods, such as aero-GaN [48], aero-ZnS [50], aero-Ga_2O_3 [51], and aero-TiO_2 [52] were developed previously on the basis of networks of ZnO microtetrapods produced by the flame transport approach [47]. Such networks of ZnO microtetrapods were used as sacrificial templates for the preparation of aero-GaN 3D structures [48].

As previously shown, Au nanodots can be deposited on semiconductor substrates by pulsed electroplating [49], and the deposition is controlled by the conductivity of the substrate, the applied cathodic voltage and the width of voltage pulses. The mechanism of pulsed electrochemical deposition of metal nanodots (the so-called "hopping electrodeposition") is governed by the Schottky barrier height at the interface of the metallic nanodot with the semiconductor template [53]. The size of the metal nanodots after their nucleation is controlled by the number of applied voltage pulses. However, it is limited by the height of the Schottky barrier. For instance, for a GaP template with the free electron concentration of 2×10^{17} cm^{-3} the limit diameter of Au dots was found to be around 20 nm [53]. After reaching this threshold size, a new nanodot is nucleated, and the deposition process continues until the entire surface of the semiconductor template is covered by a monolayer of self-assembled Au nanodots. It was also found that the

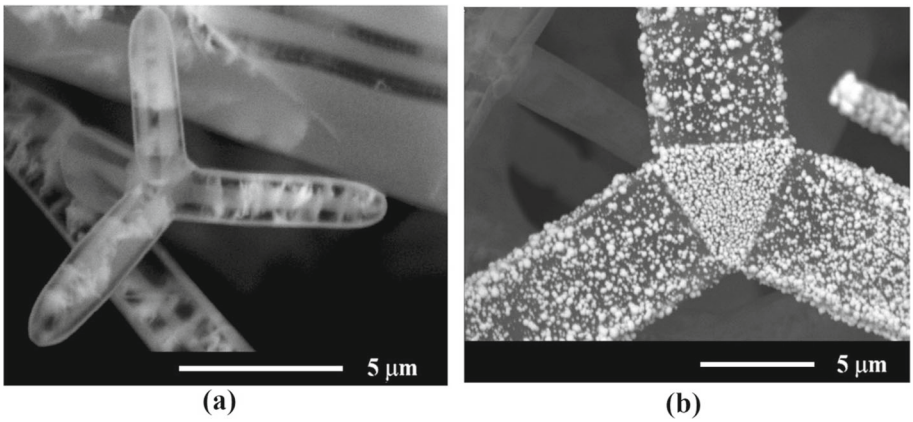

Fig. 1 **a** SEM image (registered using a detector with backscattered electrons) of a hollow GaN microtetrapod from the aero-GaN sample. **b** SEM image of a hollow GaN microtetrapod covered by Au nanodots. The parameters of electroplating: $t_{on} = 50$ μs; $t_{off} = 1$ s; $U = -15$ V, $t_{dep} = 120$ s

density of the deposited Au nanodots on semiconductor nanostructures under identical electroplating conditions is determined by the conductivity of the nanostructure, and it was proposed to use the gold electroplating as a tool for assessing the conductivity of semiconductor nanostructures [54].

SEM image of a GaN hollow microtetrapod extracted from the aero-GaN material produced as described elsewhere [48] is shown in Fig. 1a. The gold electroplating on such a microtetrapod with 50 μs pulse width resulted in its coating with Au nanodots, as shown in Fig. 1b. One can see that the density of Au nanodots deposited in the region where the microtetrapod arms intersect is higher, indicating the higher electrical conductivity of this region as compared to the conductivity of the microtetrapod arms. The deposited Au nanodots on these microstructures may serve as catalyst nucleation sites for the growth of nanowires with a given composition, which are expected to grow out from the surface of the microtetrapod arm. Thus, a complex micro-nano-architecture composed of two constituent components with different chemical compositions can be formed, namely of microtetrapods covered by an array of nanowires.

3.2 Porous microdomains prepared by design for metal deposition

The microdomains of pores with a controlled design represent another platform for the metal-assisted fabrication of complex micro-nano-architectures. It is known that two main types of pores are generated by anodization of semiconductor substrates, namely of pores growing in crystallographic directions, and of those growing in the directions of current lines. The latter ones are always oriented in a direction perpendicular to the equipotential lines inside the anodized sample, irrespective of the crystallographic orientation [55]. When the surface of the substrate subjected to anodization is covered by a mask with a special design, the current line-oriented pores start to grow on the surface of the substrate non-covered by the mask, which is exposed to the electrolyte. They are initially oriented perpendicularly to the substrate surface, but later on their growth is deflected under the mask in the direction parallel to the substrate surface [56]. The equipotential lines inside the anodized sample and, respectively, the configurations of the pore microdomains formed under the mask are determined by the design of the mask, as shown in Fig. 2a for a square mask. The different shape of the porous design at the corner marked with an asterisk in Fig. 2a as compared to the other three corners is due to the worse adhesion of the photoresist mask at this corner. The technological route for growing pores parallel to the top surface of the substrate was previously applied to InP and ZnSe templates [55, 57].

More complex designs of the microdomains of pores are produced with masks containing holes [58], as shown in Fig. 2b. A sulfur doped *n*-InP wafer with the thickness of 500 μm and electron concentration of 1.3×10^{18} cm^{-3}, was covered by a positive photoresist AZ 1505 with the thickness of 1 μm and the shape shown in Fig. 2b (left). It was subsequently subjected to anodization in darkness at room temperature in an aqueous 3.5 M NaCl solution. Two types of pore arrays are generated during anodization. One array of pores propagated under the photoresist mask from its edge in the direction of the round hole, as marked by bold arrows in Fig. 2b (right). Another array of pores started to propagate in the radial direction of the open hole in the photoresist mask as marked by narrow arrows. This second array of pores was later on deflected in the direction of the first arrays of pores due to their interaction. It is known that the current-line oriented pores cannot intersect each other, in contrast to the crystallographically-oriented pores [55]. An interesting design of the pore domain is formed as a result of this interaction, as shown in Fig. 2b (right). This design with two pore arrays formed in the same porous micro-domain is especially important for microfluidic applications, since the entrance in the first array of pores is at the edge of the photoresist mask, while the entrance in the second arrays of pores is situated in the round hole of the mask.

Another interesting feature of this microdomain of pores is related to the fact that it is buried under the surface of the semiconductor wafer at a deepness of the order of the surface depletion region, i.e., from several tens to several hundreds of nanometers, depending on the conductivity of the anodized substrate [56]. Since this region is depleted from charge carriers, its resistivity is high, and metal deposition does not occur on it upon electroplating. On the other side, the distance between pores is larger, and these regions in

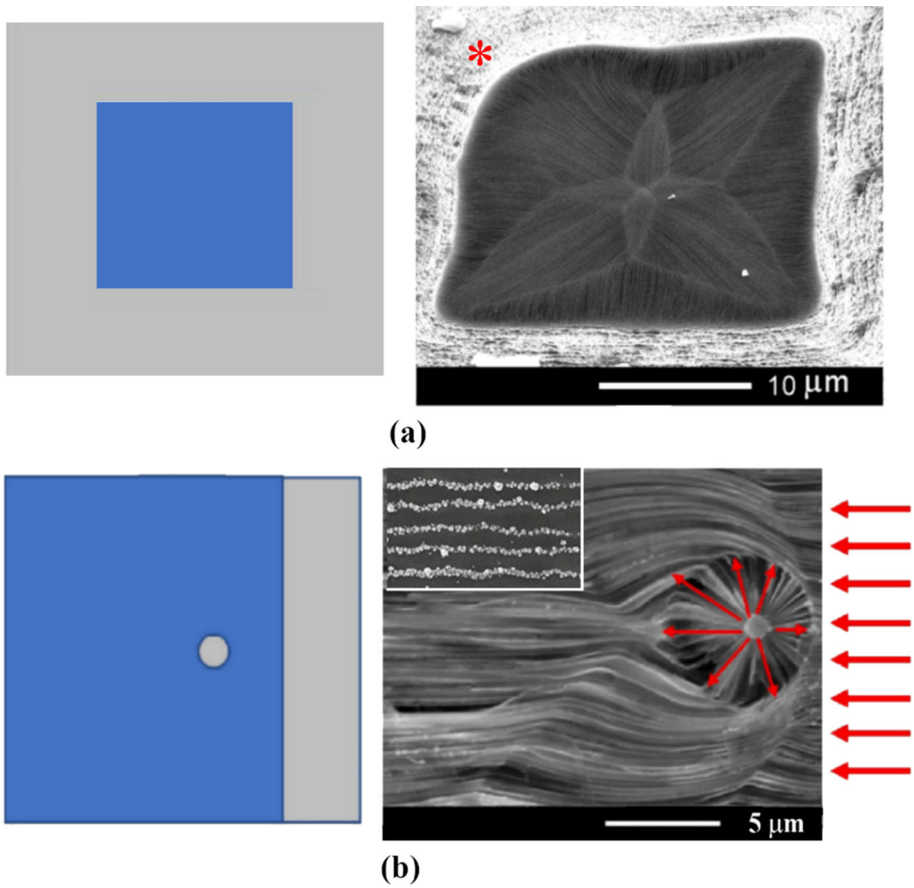

Fig. 2 **a** Top view SEM image of the porous domain formed in an InP substrate under the square photoresist mask after electrochemical etching. **b** SEM image of the anodized InP substrate using a photoresist mask with an open hole. Inset in **(b)** is the enlarged view of a region of the sample surface after pulsed electroplating: $t_{on} = 10$ µs; $t_{off} = 1$ s; $U = -12$ V, $t_{dep} = 100$ s. SEM images after electrochemical etching are reproduced from Physica Status Solidi—Rapid Research Letters 2300039. https://doi.org/10.1002/pssr.202300039. Copyright © 2023 with permission from John Wiley and Sons [58]

between pores are conductive. As a result, arrays of Au nanodots are deposited on these conductive regions during electroplating, as shown in the inset of Fig. 2b. The density of the Au nanodots in the array is controlled by the number of applied pulses during electroplating. Apart from that, Au nanodots can also be deposited inside the pores of the porous domain, and their density can be varied from rare nanodots to monolayers of self-assembled Au nanodots forming metal nanotubes inside the pores. Such a kind of metal nanotubes has been previously deposited in different porous templates [55, 57, 59]. As mentioned above, these Au nanodots can serve as catalyst nucleation sites for the growth of nanowires with various chemical compositions, forming another type of complex micro-nano-structures.

3.3 Patterned GaN substrates for the deposition of Au nanodots

GaN substrates grown by HVPE technology can also serve as a platform for the deposition by design of semiconductor nanowires. It was previously found that the HVPE grown GaN crystals are micro-structured both along the surface and in the bulk. In spite of advantages of the HVPE growth, such as high growth rate (> 100 µm/h) and relatively high material purity, producing material with uniform conductivity throughout the bulk is still a challenge. The formation of V-shaped defects or pits during the HVPE growth of GaN was found to lead generally to the generation of extended inhomogeneities upon subsequent overgrowth [60].

Pyramidal-type microstructures have been better evidenced in the HVPE grown GaN as a result of anodization of the as-grown material [60, 61], and a model has been proposed to explain their formation [60]. It was demonstrated that these pyramids consist of layers with alternating high and low conductivity [60–62], and these features result in the formation of concentric rings with alternating conductivity at the surface of the material, as shown in Fig. 3a. These circular microdomains are suitable for the deposition of metallic nanodots on rings with higher conductivity, as shown in Fig. 3b. The deposited nanodots can be further used for the growth of nanowires from other semiconductor materials, thus resulting in the fabrication of complex micro- nano-architectures similar to those produced on porous InP microdomains.

The cleavage of the electrochemically etched sample shown in Fig. 3c demonstrates the conductivity modulation in the bulk of the material, while the image in Fig. 3d demonstrates the electrochemical deposition of Au nanodots on a freshly cleaved as-grown HVPE GaN substrate.

Figure 4 demonstrates possibilities for controlling the density of the deposited Au nanodots on a GaN substrate grown by HVPE from isolated nanodots to concentric dense gold rings.

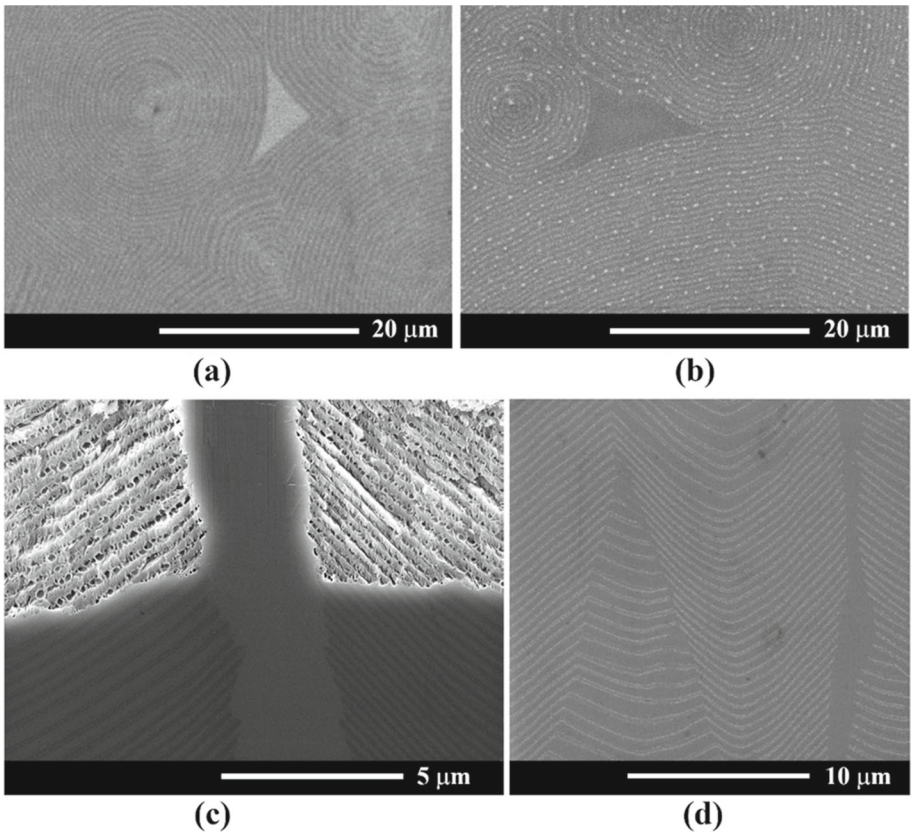

Fig. 3 **a** Top-view SEM image (registered using a detector with backscattered electrons) of the as-grown HVPE GaN free-standing substrate revealing alternating concentric rings with different electrical conductivities. The dark regions exhibit higher conductivity. **b** gold nanodots electroplated for 100 s on the surface of the HVPE as-grown GaN substrate at 50 μs pulse width, 1 s pause between the pulses, and pulse amplitude—15 V. **c** cross-sectional SEM view of HVPE GaN substrate after electrochemical etching in 1 M HNO_3 at 25 V for 10 min. **d** The electrochemical deposition of Au nanodots on freshly cleaved as-grown HVPE GaN substrate demonstrating the nonuniformity of doping during the HVPE growth

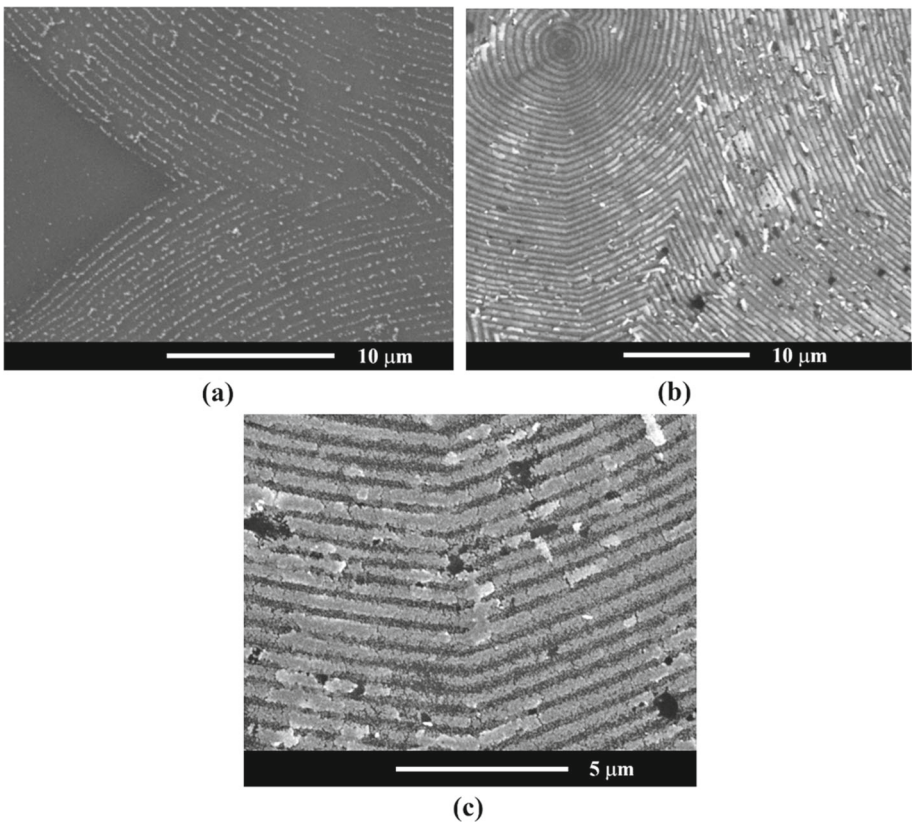

Fig. 4 Dependence of Au deposition on the electroplating conditions: **a** $t_{on} = 50$ μs; $t_{off} = 1$ s; $U = -15$ V, $t_{dep} = 100$ s; **b** at longer duration of electroplating $t_{dep} = 1200$ s; **c** enlarged SEM image from (**b**)

4 Conclusions

The results of this study demonstrate possibilities for depositing arrays of Au nanodots with controlled density on various microstructured semiconductor substrates. The density of nanodots is determined by the parameters of pulsed electroplating, such as the voltage pulse amplitude and width, the pause between pulses, as well as by the conductivity of the substrate. Networks of hollow GaN microtetrapods constituting the aero-GaN, microdomains of pores with a controlled design produced by anodization of InP substrates, and patterned microdomains composed of strips with alternating electrical conductivity inherent to HVPE-grown GaN are among microstructures demonstrated in this study. The self-assembled Au nanodots can serve as catalyst nucleation sites for the growth of nanowires with various chemical compositions, as previously demonstrated using different technological approaches, thus forming complex 3D micro-nano-architectures promising for photocatalytic [51, 63] and other applications.

Acknowledgements The authors acknowledge the research team from the Christian-Albrechts University of Kiel in Germany (R. Adelung) for providing the as-grown ZnO microtetrapods.

Funding This research was partially funded by the National Agency for Research and Development of Moldova under the Grant #20.80009.5007.20.

Data availability The data presented in this study are available on request from the corresponding author.

Declarations

Conflict of interest The authors declare no conflicts of interest. The funding sponsors had no role in the design of the study; in the collection, analyses, or interpretation of data; in the writing of the manuscript, and in the decision to publish the results.

References

1. G. Miao, D. Zhang, Stages in the catalyst-free InP nanowire growth on silicon (100) by metal organic chemical vapor deposition. Nanoscale Res. Lett. **7**, 321 (2012). https://doi.org/10.1186/1556-276X-7-321
2. J. Wang, S.R. Plissard, M.A. Verheijen, L.-F. Feiner, A. Cavalli, E.P.A.M. Bakkers, Reversible switching of InP nanowire growth direction by catalyst engineering. Nano Lett. **13**, 3802–3806 (2013). https://doi.org/10.1021/nl401767b
3. S. Bhunia, T. Kawamura, S. Fujikawa, H. Nakashima, K. Furukawa, K. Torimitsu, Y. Watanabe, Vapor–liquid–solid growth of vertically aligned InP nanowires by metalorganic vapor phase epitaxy. Thin Solid Films **464–465**, 244–247 (2004). https://doi.org/10.1016/j.tsf.2004.06.101
4. A.M. Shafi, S. Das, V. Khayrudinov, E.-X. Ding, M.G. Uddin, F. Ahmed, Z. Sun, H. Lipsanen, Direct epitaxial growth of InP nanowires on MoS2 with strong nonlinear optical response. Chem. Mater. **34**, 9055–9061 (2022). https://doi.org/10.1021/acs.chemmater.2c01602
5. J. Liu, H. Nie, B. Yan, K. Yang, H. Yang, V. Khayrudinov, H. Lipsanen, B. Zhang, J. He, Nonlinear optical absorption properties of InP nanowires and applications as a saturable absorber. Photon. Res. PRJ **8**, 1035–1041 (2020). https://doi.org/10.1364/PRJ.389669
6. A. Jaffal, P. Regreny, G. Patriarche, N. Chauvin, M. Gendry, Density-controlled growth of vertical InP nanowires on Si(111) substrates. Nanotechnology **31**, 354003 (2020). https://doi.org/10.1088/1361-6528/ab9475
7. M.H. Hadj Alouane, O. Nasr, H. Khmissi, B. Ilahi, G. Patriarche, M.M. Ahmad, M. Gendry, C. Bru-Chevallier, N. Chauvin, Temperature dependence of optical properties of InAs/InP quantum rod-nanowires grown on Si substrate. J. Lumin. **231**, 117814 (2021). https://doi.org/10.1016/j.jlumin.2020.117814
8. G. Zhang, K. Tateno, T. Sogawa, H. Gotoh, Diameter-tailored telecom-band luminescence in InP/InAs heterostructure nanowires grown on InP (111)B substrate with continuously-modulated diameter from microscale to nanoscale. Nanotechnology **29**, 155202 (2018). https://doi.org/10.1088/1361-6528/aaab17
9. K. Tateno, G. Zhang, H. Gotoh, T. Sogawa, VLS growth of alternating InAsP/InP heterostructure nanowires for multiple-quantum-dot structures. Nano Lett. **12**, 2888–2893 (2012). https://doi.org/10.1021/nl300482n
10. I. Verma, S. Salimian, V. Zannier, S. Heun, F. Rossi, D. Ercolani, F. Beltram, L. Sorba, High-mobility free-standing InSb nanoflags grown on InP nanowire stems for quantum devices. ACS Appl. Nano Mater. **4**, 5825–5833 (2021). https://doi.org/10.1021/acsanm.1c00734
11. V.G. Dubrovskii, T. Xu, A.D. Álvarez, S.R. Plissard, P. Caroff, F. Glas, B. Grandidier, Self-equilibration of the diameter of Ga-catalyzed GaAs nanowires. Nano Lett. **15**, 5580–5584 (2015). https://doi.org/10.1021/acs.nanolett.5b02226
12. S. Vorathamrong, S. Panyakeow, S. Ratanathammaphan, P. Praserthdam, Surface evolution of native silicon oxide layer and its effects on the growth of self-assisted VLS GaAs nanowires. AIP Adv. **9**, 025318 (2019). https://doi.org/10.1063/1.5084344
13. H. Küpers, R.B. Lewis, A. Tahraoui, M. Matalla, O. Krüger, F. Bastiman, H. Riechert, L. Geelhaar, Diameter evolution of selective area grown Ga-assisted GaAs nanowires. Nano Res. **11**, 2885–2893 (2018). https://doi.org/10.1007/s12274-018-1984-1
14. Y. André, K. Lekhal, P. Hoggan, G. Avit, F. Cadiz, A. Rowe, D. Paget, E. Petit, C. Leroux, A. Trassoudaine, M. Réda Ramdani, G. Monier, D. Colas, R. Ajib, D. Castelluci, E. Gil, Vapor liquid solid-hydride vapor phase epitaxy (VLS-HVPE) growth of ultra-long defect-free GaAs nanowires: Ab initio simulations supporting center nucleation. J. Chem. Phys. **140**, 194706 (2014). https://doi.org/10.1063/1.4874875
15. C. Blumberg, L. Liborius, J. Ackermann, F.-J. Tegude, A. Poloczek, W. Prost, N. Weimann, Spatially controlled VLS epitaxy of gallium arsenide nanowires on gallium nitride layers. CrystEngComm **22**, 1239–1250 (2020). https://doi.org/10.1039/C9CE01926J
16. C.B. Maliakkal, D. Jacobsson, M. Tornberg, A.R. Persson, J. Johansson, R. Wallenberg, K.A. Dick, In situ analysis of catalyst composition during gold catalyzed GaAs nanowire growth. Nat. Commun. **10**, 4577 (2019). https://doi.org/10.1038/s41467-019-12437-6
17. M. Oliva, G. Gao, E. Luna, L. Geelhaar, R.B. Lewis, Axial GaAs/Ga(As, Bi) nanowire heterostructures. Nanotechnology **30**, 425601 (2019). https://doi.org/10.1088/1361-6528/ab3209
18. J. Bauer, V. Gottschalch, H. Paetzelt, G. Wagner, VLS growth of GaAs/(InGa)As/GaAs axial double-heterostructure nanowires by MOVPE. J. Cryst. Growth **310**, 5106–5110 (2008). https://doi.org/10.1016/j.jcrysgro.2008.07.059

19. M. Scuderi, P. Prete, N. Lovergine, C. Spinella, G. Nicotra, Effects of VLS and VS mechanisms during shell growth in GaAs-AlGaAs core-shell nanowires investigated by transmission electron microscopy. Mater. Sci. Semicond. Process. **65**, 108–112 (2017). https://doi.org/10.1016/j.mssp.2016.11.018
20. D.-D. Wei, S.-X. Shi, C. Zhou, X.-T. Zhang, P.-P. Chen, J.-T. Xie, F. Tian, J. Zou, Formation of GaAs/GaSb core–shell heterostructured nanowires grown by molecular-beam epitaxy. Crystals **7**, 94 (2017). https://doi.org/10.3390/cryst7040094
21. R. Popovitz-Biro, A. Kretinin, P. Von Huth, H. Shtrikman, InAs/GaAs core–shell nanowires. Cryst. Growth Des. **11**, 3858–3865 (2011). https://doi.org/10.1021/cg200393y
22. V.V. Fedorov, Y. Berdnikov, N.V. Sibirev, A.D. Bolshakov, S.V. Fedina, G.A. Sapunov, L.N. Dvoretckaia, G. Cirlin, D.A. Kirilenko, M. Tchernycheva, I.S. Mukhin, Tailoring morphology and vertical yield of self-catalyzed GaP nanowires on template-free Si substrates. Nanomaterials **11**, 1949 (2021). https://doi.org/10.3390/nano11081949
23. G. Zhang, K. Tateno, T. Sogawa, H. Nakano, Growth and characterization of GaP nanowires on Si substrate. J. Appl. Phys. **103**, 014301 (2008). https://doi.org/10.1063/1.2828165
24. J.P. Boulanger, R.R. LaPierre, Patterned gold-assisted growth of GaP nanowires on Si. Semicond. Sci. Technol. **27**, 035002 (2012). https://doi.org/10.1088/0268-1242/27/3/035002
25. M. Steidl, M. Wu, K. Peh, P. Kleinschmidt, E. Spiecker, T. Hannappel, Impact of N incorporation on VLS growth of GaP(N) nanowires utilizing UDMH. Nanoscale Res. Lett. **13**, 417 (2018). https://doi.org/10.1186/s11671-018-2833-6
26. S. Lee, W. Wen, Q. Cheek, S. Maldonado, Comparison of GaP nanowires grown from Au and Sn vapor–liquid–solid catalysts as photoelectrode materials. J. Cryst. Growth **482**, 36–43 (2018). https://doi.org/10.1016/j.jcrysgro.2017.10.021
27. M. Hocevar, G. Immink, M. Verheijen, N. Akopian, V. Zwiller, L. Kouwenhoven, E. Bakkers, Growth and optical properties of axial hybrid III–V/silicon nanowires. Nat. Commun. **3**, 1266 (2012). https://doi.org/10.1038/ncomms2277
28. M. Steidl, K. Schwarzburg, B. Galiana, T. Kups, O. Supplie, P. Kleinschmidt, G. Lilienkamp, T. Hannappel, MOVPE growth of GaP/GaPN core–shell nanowires: N incorporation, morphology and crystal structure. Nanotechnology **30**, 104002 (2019). https://doi.org/10.1088/1361-6528/aaf607
29. V. Purushothaman, V. Ramakrishnan, K. Jeganathan, Interplay of VLS and VS growth mechanism for GaN nanowires by a self-catalytic approach. RSC Adv. **2**, 4802–4806 (2012). https://doi.org/10.1039/C2RA01000C
30. A. Waseem, M.A. Johar, M.A. Hassan, I.V. Bagal, A. Abdullah, J.-S. Ha, J.K. Lee, S.-W. Ryu, GaN nanowire growth promoted by In–Ga–Au alloy catalyst with emphasis on agglomeration temperature and in composition. ACS Omega **6**, 3173–3185 (2021). https://doi.org/10.1021/acsomega.0c05587
31. A. Rothman, J. Maniš, V.G. Dubrovskii, T. Šikola, J. Mach, E. Joselevich, Kinetics of guided growth of horizontal GaN nanowires on flat and faceted sapphire surfaces. Nanomaterials **11**, 624 (2021). https://doi.org/10.3390/nano11030624
32. M. Zervos, A. Othonos, Gallium hydride vapor phase epitaxy of GaN nanowires. Nanoscale Res. Lett. **6**, 262 (2011). https://doi.org/10.1186/1556-276X-6-262
33. K.-L. Wu, Y. Chou, C.-C. Su, C.-C. Yang, W.-I. Lee, Y.-C. Chou, Controlling bottom-up rapid growth of single crystalline gallium nitride nanowires on silicon. Sci. Rep. **7**, 17942 (2017). https://doi.org/10.1038/s41598-017-17980-0
34. A. Abdullah, M.A. Kulkarni, H. Thaalbi, F. Tariq, S.-W. Ryu, Epitaxial growth of 1D GaN-based heterostructures on various substrates for photonic and energy applications. Nanoscale Adv. **5**, 1023–1042 (2023). https://doi.org/10.1039/D2NA00711H
35. G. Zhu, Y. Zhou, S. Wang, R. Yang, Y. Ding, X. Wang, Y. Bando, Z. Lin Wang, Synthesis of vertically aligned ultra-long ZnO nanowires on heterogeneous substrates with catalyst at the root. Nanotechnology **23**, 055604 (2012). https://doi.org/10.1088/0957-4484/23/5/055604
36. K. Govatsi, A. Chrissanthopoulos, V. Dracopoulos, S.N. Yannopoulos, The influence of Au film thickness and annealing conditions on the VLS-assisted growth of ZnO nanostructures. Nanotechnology **25**, 215601 (2014). https://doi.org/10.1088/0957-4484/25/21/215601
37. C. Baratto, M. Ferroni, E. Comini, G. Faglia, S. Kaciulis, S.K. Balijepalli, G. Sberveglieri, Vapour phase nucleation of ZnO nanowires on GaN: growth habit, interface study and optical properties. RSC Adv. **6**, 15087–15093 (2016). https://doi.org/10.1039/C5RA25019F
38. Y. Kawai, M. Sakai, K. Hara, T. Kouno, Selectively enhanced microarea crystal growth of ZnO nano- and microwires on GaN on sapphire substrates by mist chemical vapor deposition. J. Ceram. Soc. Jpn. **130**, 857–860 (2022). https://doi.org/10.2109/jcersj2.22060
39. O.W. Kennedy, E.R. White, M.S.P. Shaffer, P.A. Warburton, Vapour–liquid–solid growth of ZnO-ZnMgO core–shell nanowires by gold-catalysed molecular beam epitaxy. Nanotechnology **30**, 194001 (2019). https://doi.org/10.1088/1361-6528/ab011c
40. M. Lin, T. Sudhiranjan, C. Boothroyd, K.P. Loh, Influence of Au catalyst on the growth of ZnS nanowires. Chem. Phys. Lett. **400**, 175–178 (2004). https://doi.org/10.1016/j.cplett.2004.10.115
41. M. Hafeez, S. Rehman, U. Manzoor, M.A. Khan, A.S. Bhatti, Catalyst driven optical properties of the self-assembled ZnS nanostructures. Phys. Chem. Chem. Phys. **15**, 9726–9734 (2013). https://doi.org/10.1039/C3CP50534K
42. Q. An, X. Meng, K. Xiong, Y. Qiu, W. Lin, One-step fabrication of single-crystalline ZnS nanotubes with a novel hollow structure and large surface area for photodetector devices. Nanotechnology **28**, 105502 (2017). https://doi.org/10.1088/1361-6528/28/10/105502
43. S. Kumar, F. Fossard, G. Amiri, J.-M. Chauveau, V. Sallet, MOCVD growth and structural properties of ZnS nanowires: a case study of polytypism. Nanomaterials **12**, 2323 (2022). https://doi.org/10.3390/nano12142323
44. J.H. Kim, S.C. Kim, D.H. Kim, K.H. Oh, W.-K. Hong, T.-S. Bae, H.-S. Chung, Fabrication and characterization of ZnS/diamond-like carbon core–shell nanowires. J. Nanomater. **2016**, e4726868 (2016). https://doi.org/10.1155/2016/4726868
45. D. Moore, J.R. Morber, R.L. Snyder, Z.L. Wang, Growth of ultralong ZnS/SiO_2 Core−shell nanowires by volume and surface diffusion VLS process. J. Phys. Chem. C **112**, 2895–2903 (2008). https://doi.org/10.1021/jp709903b
46. E. Butanovs, A. Kuzmin, S. Piskunov, K. Smits, A. Kalinko, B. Polyakov, Synthesis and characterization of GaN/ReS2, ZnS/ReS2 and ZnO/ReS2 core/shell nanowire heterostructures. Appl. Surf. Sci. **536**, 147841 (2021). https://doi.org/10.1016/j.apsusc.2020.147841
47. Y.K. Mishra, S. Kaps, A. Schuchardt, I. Paulowicz, X. Jin, D. Gedamu, S. Freitag, M. Claus, S. Wille, A. Kovalev, S.N. Gorb, R. Adelung, Fabrication of macroscopically flexible and highly porous 3D semiconductor networks from interpenetrating nanostructures by a simple flame transport approach. Part. Part. Syst. Charact. **30**, 775–783 (2013). https://doi.org/10.1002/ppsc.201300197
48. I. Tiginyanu, T. Braniste, D. Smazna, M. Deng, F. Schütt, A. Schuchardt, M.A. Stevens-Kalceff, S. Raevschi, U. Schürmann, L. Kienle, N.M. Pugno, Y.K. Mishra, R. Adelung, Self-organized and self-propelled aero-GaN with dual hydrophilic-hydrophobic behaviour. Nano Energy **56**, 759–769 (2019). https://doi.org/10.1016/j.nanoen.2018.11.049
49. E.I. Monaico, E.V. Monaico, V.V. Ursaki, I.M. Tiginyanu, Controlled electroplating of noble metals on III–V semiconductor nanotemplates fabricated by anodic etching of bulk substrates. Coatings **12**, 1521 (2022). https://doi.org/10.3390/coatings12101521
50. I. Plesco, T. Braniste, N. Wolff, L. Gorceac, V. Duppel, B. Cinic, Y.K. Mishra, A. Sarua, R. Adelung, L. Kienle, I. Tiginyanu, Aero-ZnS architectures with dual hydrophilic-hydrophobic properties for microfluidic applications. APL Mater. **8**, 061105 (2020). https://doi.org/10.1063/5.0010222
51. I. Plesco, V. Ciobanu, T. Braniste, V. Ursaki, F. Rasch, A. Sarua, S. Raevschi, R. Adelung, J. Dutta, I. Tiginyanu, Highly porous and ultra-lightweight aero-Ga_2O_3: enhancement of photocatalytic activity by noble metals. Materials **14**, 1985 (2021). https://doi.org/10.3390/ma14081985

52. V. Ciobanu, V.V. Ursaki, S. Lehmann, T. Braniste, S. Raevschi, V.V. Zalamai, E.V. Monaico, P. Colpo, K. Nielsch, I.M. Tiginyanu, Aero-TiO_2 prepared on the basis of networks of ZnO tetrapods. Crystals **12**, 1753 (2022). https://doi.org/10.3390/cryst12121753
53. I. Tiginyanu, E. Monaico, K. Nielsch, Self-assembled monolayer of Au nanodots deposited on porous semiconductor structures. ECS Electrochem. Lett. **4**, D8 (2015). https://doi.org/10.1149/2.0041504eel
54. E.V. Monaico, I.M. Tiginyanu, V.V. Ursaki, K. Nielsch, D. Balan, M. Prodana, M. Enachescu, Gold electroplating as a tool for assessing the conductivity of InP nanostructures fabricated by anodic etching of crystalline substrates. J. Electrochem. Soc. **164**, D179 (2017). https://doi.org/10.1149/2.1071704jes
55. E. Monaico, I. Tiginyanu, V. Ursaki, Porous semiconductor compounds. Semicond. Sci. Technol. **35**, 103001 (2020). https://doi.org/10.1088/1361-6641/ab9477
56. E. Monaico, E.I. Monaico, V.V. Ursaki, I.M. Tiginyanu, K. Nielsch, Electrochemical deposition by design of metal nanostructures. Surf. Eng. Appl. Electrochem. **55**, 367–372 (2019). https://doi.org/10.3103/S1068375519040070
57. I.M. Tiginyanu, V.V. Ursaki, E. Monaico, M. Enachi, V.V. Sergentu, G. Colibaba, D.D. Nedeoglo, A. Cojocaru, H. Föll, Quasi-ordered networks of metal nanotubes embedded in semiconductor matrices for photonic applications. J. Nanoelectron. Optoelectron. **6**, 463–472 (2011). https://doi.org/10.1166/jno.2011.1197
58. E.V. Monaico, E.I. Monaico, V.V. Ursaki, I.M. Tiginyanu, Porous semiconductor compounds with engineered morphology as a platform for various applications. Phys. Status Solidi Rapid Res. Lett. (2023). https://doi.org/10.1002/pssr.202300039
59. I. Tiginyanu, E. Monaico, E. Monaico, Ordered arrays of metal nanotubes in semiconductor envelope. Electrochem. Commun. **10**, 731–734 (2008). https://doi.org/10.1016/j.elecom.2008.02.029
60. I. Tiginyanu, M.A. Stevens-Kalceff, A. Sarua, T. Braniste, E. Monaico, V. Popa, H.D. Andrade, J.O. Thomas, S. Raevschi, K. Schulte, R. Adelung, Self-organized three-dimensional nanostructured architectures in bulk GaN generated by spatial modulation of doping. ECS J. Solid State Sci. Technol. **5**, P218 (2016). https://doi.org/10.1149/2.0091605jss
61. E. Monaico, C. Moise, G. Mihai, V.V. Ursaki, K. Leistner, I.M. Tiginyanu, M. Enachescu, K. Nielsch, Towards uniform electrochemical porosification of bulk HVPE-grown GaN. J. Electrochem. Soc. **166**, H3159 (2019). https://doi.org/10.1149/2.0251905jes
62. N. Wolff, P. Jordt, T. Braniste, V. Popa, E. Monaico, V. Ursaki, A. Petraru, R. Adelung, B.M. Murphy, L. Kienle, I. Tiginyanu, Modulation of electrical conductivity and lattice distortions in bulk HVPE-grown GaN. ECS J. Solid State Sci. Technol. **8**, Q141 (2019). https://doi.org/10.1149/2.0041908jss
63. N. Wolff, V. Ciobanu, M. Enachi, M. Kamp, T. Braniste, V. Duppel, S. Shree, S. Raevschi, M. Medina-Sánchez, R. Adelung, O.G. Schmidt, L. Kienle, I. Tiginyanu, Advanced hybrid GaN/ZnO nanoarchitectured microtubes for fluorescent micromotors driven by UV light. Small **16**, 1905141 (2020). https://doi.org/10.1002/smll.201905141